Ecological Indicators 177 (2025) 113652

Contents lists available at ScienceDirect

Ecological Indicators

journal homepage: www.elsevier.com/locate/ecolind

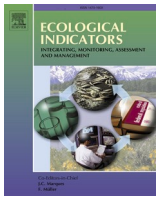

Original Articles

Long-term effects of forest growth dynamics and climate change on groundwater recharge and evapotranspiration in a steep catchment of western Japan

Rendilicha Halake Guyo [a,b], Kunyang Wang [c], Shin-ichi Onodera [c], Mitsuyo Saito [c,*], Toshitsugu Moroizumi [a]

[a] Graduate School of Environmental and Life Science, Okayama University, 3-1-1 Tsushima-naka, Kita-ku, Okayama-city, Okayama 700-8530, Japan
[b] Department of Soil, Water and Environmental Engineering, Jomo Kenyatta University of Agriculture and Technology, P.O. BOX 62000-00200, Nairobi, Kenya
[c] Graduate School of Advanced Science and Engineering, Hiroshima University, 1-7-1 Kagamiyama, Higashi-Hiroshima, Hiroshima 739-8521, Japan

ARTICLE INFO

Keywords:
Forest growth
SWAT
Groundwater recharge
Evapotranspiration
MODIS LAI
PML_V2
Climate change

ABSTRACT

Growing water demand for human and environmental needs has led to increased reliance on groundwater resources. However, groundwater is a finite resource, and its sustainability is closely linked to recharge processes, which are influenced by forest growth dynamics as well as climate change. Evapotranspiration, largely driven by vegetation cover and climatic conditions, represents a major component of terrestrial water loss that can reduce groundwater recharge. In this study, forest growth trends, reflecting the complete developmental stages from juvenile to post-maturity of a representative species, were reconstructed using remote sensing data, forest inventories, and field studies, and incorporated into the SWAT model to evaluate their impacts on groundwater recharge and evapotranspiration as indicators of forest hydrological function and ecosystem health. The model's vegetation growth simulation was enhanced and uncertainty reduced by dynamically updating it with MODIS-derived leaf area index (LAI) at 5-year intervals. Groundwater recharge estimates were further improved through multi-variable calibration using Penman–Monteith–Leuning evapotranspiration (V2) and streamflow data to ensure water budget closure. Results showed that evergreen conifer growth from planting to maturity significantly reduced groundwater recharge (–4.7 mm/year) and increased evapotranspiration (+7.6 mm/year). In contrast, natural and mature deciduous broadleaf forests showed more stable recharge and evapotranspiration trends. Rising temperatures were identified as a key climatic driver of reduced recharge and increased evapotranspiration, reflecting broader global warming impacts. This study demonstrates that forest growth dynamics, especially during the critical transition from planting to maturity, alongside climate change, play a crucial role in shaping the catchment's water balance and offer valuable insights for sustainable groundwater management, particularly in transitional forest ecosystems.

1. Introduction

Groundwater, the major freshwater store on Earth, is crucial to the global water cycle and provides potable water for billions of people around the world (Koirala et al., 2014; Kuang et al., 2024). However, groundwater is not an infinite resource; its sustenance hinges on groundwater recharge (GWR). Insufficient GWR can lead to reduced groundwater storage, threatening the long-term sustainability of groundwater aquifers (De Vries & Simmers, 2002). Conversely, evapotranspiration (ET), which accounts for a significant portion of terrestrial water loss, can influence water yield and diminish GWR (Bosch & Hewlett, 1982; Yang et al., 2023).

The GWR and ET processes are primarily driven by climate and vegetation cover (Natkhin et al., 2012; Simic et al., 2014; Liu et al., 2020; Rendilicha et al., 2024). The impacts of climate change and land cover conversion on these processes are widely discussed topics, with substantial improvements in understanding their effects on water availability (Cuthbert et al., 2019; Mensah et al., 2022; Wang et al., 2022a). For instance, climate change, particularly alterations in precipitation patterns and rising air temperatures, directly affects GWR

* Corresponding author.
E-mail address: misaito@hiroshima-u.ac.jp (M. Saito).

https://doi.org/10.1016/j.ecolind.2025.113652
Received 18 February 2025; Received in revised form 21 May 2025; Accepted 21 May 2025
Available online 26 June 2025
1470-160X/© 2025 The Author(s). Published by Elsevier Ltd. This is an open access article under the CC BY-NC-ND license (http://creativecommons.org/licenses/by-nc-nd/4.0/).

(Kumar, 2012). Increased ET can account for the loss of up to 40–70 % of precipitation in temperate regions and over 90 % in arid areas (Flerchinger et al., 1996; Jasechko et al., 2013), causing substantial water loss before groundwater aquifers are recharged. Previous studies have shown that converting grasslands and croplands into forests can decrease water yield (Bosch & Hewlett, 1982; Brown et al., 2005), likely due to forests having higher ET rates and enhanced rainfall infiltration, which reduce surface runoff (Bruijnzeel, 2004). Similarly, Kimbi et al. (2024) demonstrated that the conversion of paddy fields to residential areas in a suburban Japanese catchment led to a 34.9 % reduction in GWR, driven by increased impervious surfaces that limited infiltration.

In recent years, the focus has shifted toward investigating quantitative changes in land cover types, such as forests and urban areas, moving beyond traditional qualitative analyses of areal changes and distinguishing these from the effects of climate change on the water balance. For instance, Natkhin et al. (2012) examined the influence of forest age distributions on a basin's water balance and differentiated these effects from those of climate change on declining groundwater levels in Germany. Wang et al. (2021a) investigated the impact of increased impervious surface percentage in urban regions on the regional water balance, concluding that the proportion of impervious surfaces had a more profound impact on hydrological dynamics than urban expansion alone. These studies highlight the need to assess the impact of environmental changes on the water balance beyond simple qualitative evaluations.

Forest ecosystems have undergone significant changes due to elevated CO_2 levels (Yao et al., 2024), nitrogen deposition (Aber et al., 1989), historical disturbances such as World War II, and evolving forest management practices (Nita et al., 2018). These changes are particularly evident in Japan, where extensive forest destruction occurred during World War II, and 67 % of forests are now owned and managed by public and private sectors for timber production. These sectors maintain an average forest age of 40 years, resulting in considerable variability across transitional forest ecosystems (Hirata et al., 2006). Such shifts influence GWR and ET over the long term (Goeking & Tarboton, 2020; Wang et al., 2022a; Hou et al., 2023). However, few long-term studies have comprehensively assessed forest ecosystems by integrating key forest growth attributes, such as species composition, LAI, biomass accumulation, and ET, especially during the critical transition period from planting to maturity. This developmental stage plays a crucial role in shaping the water balance, (Haas et al., 2022a, 2022b; Wang et al., 2022a) but remains underexplored at large spatiotemporal scales. Moreover, most past studies have been limited to specific periods within the forest development timeline, or failing to capture the complete growth process, particularly in the pre-remote sensing era, due to the lack of continuous, spatially extensive historical data (Simic et al., 2014; Wang et al., 2022a).

Studies have suggested that concurrent changes in LAI with forest growth are responsible for dynamic shifts in forest hydrological fluxes (Haydon et al., 1997; Watson et al., 1999), owing to the dependence of interception and transpiration processes on LAI. The annual LAI serves as a key indicator of forest canopy coverage, with the difference between its highest and lowest values reflecting seasonal phenology (Smettem et al., 2013). Additionally, LAI increases rapidly in the initial growth stage and peaks during juvenility, then gradually declines until maturity, though it may increase again as forests age further. These annual variations in LAI, as observed under natural conditions, serve as reliable indicators of forest age (Zhao et al., 2021), thereby enabling long-term representation of forest growth and its implications for water balance dynamics.

Over the past two decades, rapid advancements in remote sensing technologies have encouraged researchers to explore the relationship between forest structural characteristics and remotely sensed data, enabling the estimation of LAI across extensive spatiotemporal scales (Simic et al., 2014; Wang et al., 2022a). Additionally, the development of surface energy balance models has made it possible to use remote sensing for the spatial quantification and analysis of the ET process at various scales, including catchment, regional, and global levels (McShane et al., 2017). This progression addresses a longstanding challenge in hydrological research by offering deeper insights into the interactions between forest dynamics and hydrological processes (Fassnacht et al., 2024).

Building on these technological advancements, process-based hydrological models have become indispensable tools for long-term investigations of forest–hydrology interactions, particularly in data-scarce environments. Among these, the Soil and Water Assessment Tool (SWAT) (Neitsch et al., 2011) has emerged as one of the most extensively applied watershed-scale models, offering robust capabilities for simulating hydrological processes beyond the limitations of field-based measurements. Notably, SWAT facilitates retrospective analyses by integrating contemporary periods of data richness with historical conditions characterized by limited observational records, thereby enabling comprehensive assessments of long-term hydro-environmental dynamics (Golden et al., 2016; Wang et al., 2021b, 2022b; Wang et al., 2022a).

The main objective of this study is to improve the simulation of long-term forest growth trends and their impacts on hydrological processes, with particular focus on the critical transition period from planting to maturity. Towards this, forest growth trends covering complete developmental stages from juvenile to post-maturity of a representative species were reconstructed using remote sensing data, forest inventories, and previous studies. These were integrated into the SWAT model to evaluate their influence on GWR and ET as indicators of forest hydrological function and ecosystem health. The study further distinguishes the hydrological effects of forest growth from those of climate change, and enhances GWR estimation by multi-calibrating water balance components using MODIS-LAI, PML-V2 ET, and streamflow data to ensure water budget closure.

2. Materials and methods

2.1. Study area

The Asahi River Catchment (Fig. 1a), located in the central region of Okayama Prefecture in western Japan, covers an area of approximately 1,630 km^2. The catchment receives an average annual precipitation of approximately 1,500 mm; the average temperature in the region is 14.6 °C over the past 50 years. Precipitation is latitude-dependent, increasing from the downstream to upstream areas in the Chugoku Mountain ranges (Fig. 1a). The terrain within the catchment features steep slopes ranging from 0° to 58°, with elevations varying from sea level (0 m) to 1,200 m in the northern mountainous areas. This diverse topography contributes to the dynamic hydrological processes in the catchment. The catchment experiences periodic occurrence of snowfall, which is more prevalent in the upstream areas during winter, contributing to seasonal variations in the water flow and runoff patterns, thereby affecting the overall hydrology of the catchment (Rendilicha et al., 2024; Nang et al., 2024).

In Japan, particularly in the Asahi River Catchment, approximately 80 % of the forest area has remained stable for over 40 years (Hirata et al., 2006; Rendilicha et al., 2024). The increase in the demand for timber for construction after World War II led to the conversion of natural forests to coniferous plantation forests, between the 1950s and 1970s, with Sugi (*Cryptomeria japonica*) and Hinoki Cypress (*Chamaecyparis obtusa*) being the dominant species (Hirata et al., 2006; Okayama Forest Statistics, 2021). At present, about 60 % of the forest species are evergreen coniferous species, with the remaining being naturally growing mature broadleaved species (Okayama Forest Statistics, 2021) (Fig. 1b). The catchment exhibits a variety of thin and immature soil types covering the steep slopes, with Humic Cambisols being the dominant type (71 %), followed by Haplic Andosols (14 %), Fluvic Gleysols (9 %), and other soil types (6 %) (Shimizu et al., 2011) (Fig. 1c).

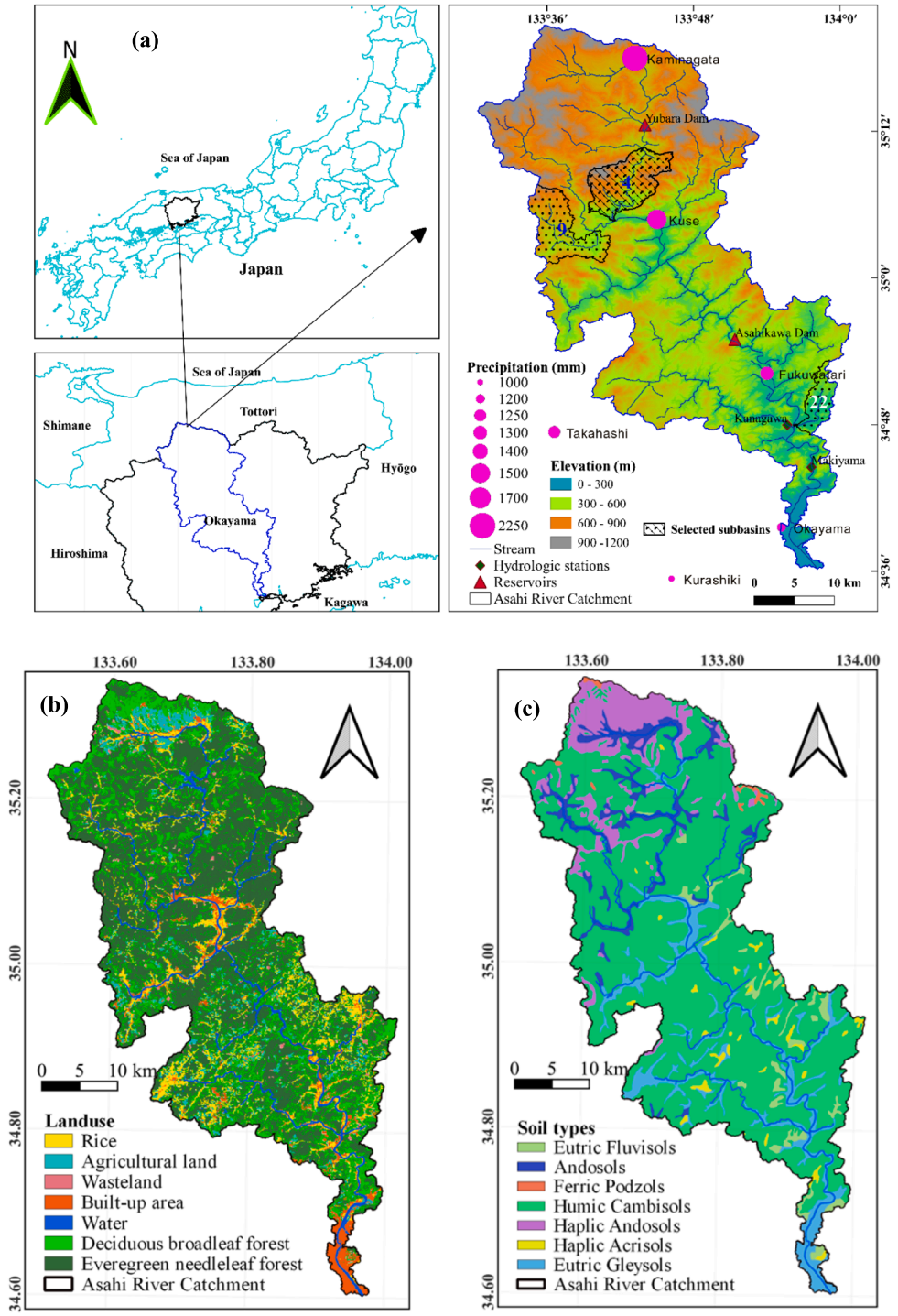

Fig. 1. Map of the Asahi River Catchment: (a) locations of meteorological stations (indicating precipitation levels, reservoirs, hydrological stations, selected sub-basins for lead area index (LAI) and evapotranspiration (ET) data collection, and elevation; (b) land use and cover map; and (c) soil map.

The catchment also includes two major reservoirs located in the upstream and downstream areas, which interrupt the natural flow of the rivers (Rendilicha et al., 2024) (Fig. 1a).

2.2. Soil and water assessment tool (SWAT)

The SWAT (Arnold et al., 1998) is a large-scale, process-based river basin model developed to quantify the impacts of land management practices on hydrological processes within complex watersheds. The model operates on a daily time step and integrates weather data, soil physical properties, topography, plant growth, and management practices to simulate catchment water balance, sediment and nutrient transport, and vegetation growth over the long term. The model computes hydrological processes using the water balance equation [Eq. (1)] (Neitsch et al., 2011).

$$SW_t = SW_o + \sum_{i=1}^{t}(R_{day} - Q_{surf} - ET_a - W_{seep} - Q_{gw}) \quad (1)$$

where SW_t is the final soil water content (mm H_2O), SW_o is the initial soil water content (mm H_2O), t is the time (days), R_{day} denotes the

precipitation on day i (mm H_2O), Q_{surf} denotes the surface runoff on day i (mm), ET_a is the evapotranspiration on day i (mm H_2O), W_{seep} is the percolation and bypass exiting the soil profile bottom on day i (mm H_2O), and Q_{gw} is the shallow groundwater discharge (return flow) on day i (mm H_2O). In the SWAT model, surface runoff (Q_{surf}) is estimated using the modified soil conservation service (SCS) curve number (CN) method. This method accounts for the initial abstraction and runoff CNs based on the soil type, land cover, and antecedent moisture conditions. After accounting for infiltration and soil moisture retention, it can estimate the amount of precipitation that generates runoff (Neitsch et al., 2011).

The SWAT model utilizes the Penman–Monteith method, among others, to calculate potential ET, from which actual evapotranspiration (ETa) is estimated based on environmental conditions, as applied in this study (Neitsch et al., 2011). The method incorporates meteorological inputs, such as temperature, humidity, wind speed, and solar radiation, to estimate the maximum amount of water that vegetation can evaporate and transpire under specific environmental conditions, with the LAI and canopy height playing a critical role in calculating both canopy and aerodynamic resistance (Neitsch et al., 2011).

In SWAT, plant growth dynamics are modeled using a simplified version of the Environmental Policy Integrated Climate (EPIC) (Neitsch et al., 2011) model to simulate leaf area development, light interception, and the conversion of intercepted light into biomass, determined by species-specific radiation-use efficiency. The tree's intra- and inter-annual growth is represented by changes in stand biomass, canopy cover and height, leaf litter, residue, and root distributions, all influenced by the LAI, potential heat units (PHU), and maturity years. Among these factors, LAI plays the most critical role in determining the amount of daily solar radiation, a major control on water movement in the land phase of the hydrologic cycle, intercepted by the leaf area. LAI is also useful in evaluating vegetation-water interactions, including water interception, transpiration rates, and soil infiltration capacity. The model employs the accumulated heat unit (PHU) theory to calculate the plant's phenological stages, specifically seasonal LAI, while accounting for factors such as water availability, temperature fluctuations, and soil nutrient levels, as expressed in Equation (2):

$$LAI = \left(\frac{yr_{cur}}{yr_{fulldev}}\right) \cdot LAI_{mx} \cdot \left(\frac{1 - fr_{PHU}}{1 - fr_{PHU,sen}}\right),\ fr_{PHU} > fr_{PHU,sen} \quad (2)$$

where LAI is the leaf area index for a given day, LAI_{mx} is the annual maximum LAI, fr_{PHU} is the fraction of potential heat units accumulated for the plant on a given day in the growing season, $fr_{PHU,\ sen}$ is the fraction of the growing season (PHU) at which senescence becomes the dominant growth process, yr_{cur} is the number of years of development the tree has accrued (years), and $yr_{fulldev}$ is the number of years for the tree species to reach full development (maturity years – MAT_YRS). Along with the MAT_YRS parameter and the biomass of a fully-developed tree (BMX_TREES) defined in the plant database, tree growth within a single year is limited to a fixed amount determined by the age of the tree relative to the number of years required for the tree species to reach full development. In this study, these parameters (MAT_YRS, BMX_TREES) were inferred from previous studies (Haas et al., 2022a).

The water that exits the bottom of the soil profile (W_{seep}) contributes to both shallow recharge (unconfined aquifers that discharge into rivers) and deep recharge (confined aquifers), based on the hydraulic properties of geological formations in the vadose zone and the aquifer percolation coefficients, respectively (Neitsch et al., 2011). In this study, the amount of GWR contributing to the groundwater flow (referred to as baseflow in some studies, e.g., Haas et al., 2022a) was considered to reflect the effect of forest growth, as this flow typically originates from shallow aquifers accessible to the roots of forest trees, allowing them to extract water through the "revap" process. For additional information on the SWAT model, please refer to the theoretical documentation presented by Neitsch et al. (2011).

2.3. Historical forest growth estimation and its representation in SWAT model

Forest species information essential for simulating growth is stored in the SWAT plant database and includes parameters that describe intra-annual forest dynamics driven by daily accumulated heat units, as well as inter-annual growth controlled by the age of the forest stand. Forest age-related growth parameters, particularly the LAI, are crucial for simulating long-term changes in forest structure and their impact on watershed hydrology.

The use of combined multi-source land use datasets has been shown to effectively enhance both the quality of input data and model accuracy (Wang et al., 2022c; 2024). In the present study, forests were categorized at the HRU level into two dominant types: deciduous broadleaf (FODB) and evergreen coniferous (FOEN), which together accounted for nearly 80 % of the study area (Fig. 1b). Detailed historical data on major reforestation initiatives and the percentage composition of planted forests within the catchment were obtained from forest inventories conducted in Okayama Prefecture, Japan. The FODB type is primarily dominated by *Quercus serrata* (Japanese Oak), while the FOEN type is largely composed of *Pinus densiflora* (Japanese Red Pine), with additional contributions from species such as *Cryptomeria japonica* (Japanese Cedar), *Chamaecyparis obtusa* (Japanese Cypress), *Tsuga diversifolia* (Japanese Hemlock), and small patches of evergreen broadleaf species, notably *Quercus acuta* (Japanese Evergreen Oak) (Okayama Forest Statistics, 2021).

Relevant parameters for simulating LAI and biomass for each forest type were identified through literature review and analysis of remote sensing data (see Table 1). These parameters include those that define leaf area development during the growing season (FRGW1, LAIMX1, FRGRW2, LAIMX2, BLAI, and DLAI), govern the conversion of intercepted light into biomass (BIO_E, T_OPT, T_BASE, and BIO_LEAF), and control light and radiation interception (LAI and EXT_COEF) (Neitsch et al., 2011).

Homogeneous sample sites for FODB and FOEN forest types were selected at the HRU level ($\geq$0.25 km^2) within selected subbasins (Fig. 1), based on the availability of sufficiently large HRUs. From these sites, MODIS-derived four-day LAI composites and PML_V2-derived eight-day ET data at 500 m resolution were extracted. As part of the quality control process, only LAI values derived from the main radiative transfer method were retained using the MODIS Quality Control (QC) mask, while retrievals from the empirical backup method were excluded to minimize uncertainties associated with low-quality observations. Missing LAI values were filled using linear interpolation. The Breaks For Additive Season and Trend (BFAST) method (Verbesselt et al., 2010) was applied to smooth noise in the LAI time series, and the annual maximum LAI, representing forest growth, was subsequently calculated.

Since inter-annual changes in LAI are a reliable indicator of forest stand age (Zhao et al., 2021), the LAI of FOEN species at the time of transplanting in the mid-1950s and at approximately 15 years of age was estimated based on published data (Ishii et al., 1999). These estimates were combined with MODIS-derived annual maximum LAI data spanning 20 years (2002–2021) to reconstruct annual maximum LAI back to 1955, resulting in a continuous 67-year time series (Fig. 2). For the naturally growing mature FODB type, the 20 years of MODIS-derived annual maximum LAI were interpolated back to the mid-1950s. A similar approach was applied by Natkhin et al. (2012), in which tree ages were reconstructed in 10-year intervals, dating back to 1955, for a forested area in Germany using age conditions from a reference year of 2006.

2.4. Scenarios set-up

Two scenarios were considered in forest areas to evaluate the effect

Table 1
Key parameters of forest growth and biomass simulation used in SWAT, derived from the literature and remote sensing, and corresponding default values before calibration.

Name	Description	Evergreen conifers (default)	Deciduous broadleaf (default)	References
FRGRW1	Heat unit of 1st point on the optimal leaf area development curve	0.02 (0.15)	0.02 (0.05)	MODIS
LAIMX1	LAI of 1st point on the optimal leaf area development curve	0.8 (0.7)	0.12 (0.05)	MODIS
FRGRW2	Heat units of 2nd point on the optimal leaf area development curve	0.08 (0.25)	0.19 (0.4)	MODIS
LAIMX2	LAI of 2nd point on the optimal leaf area development curve	0.95 (0.99)	0.95 (0.95)	MODIS
T_OPT	Optimal temperature for forest growth (°C)	26 (30)	28 (30)	Wang et al., (2022a)
T_Base	Minimum temperature for forest growth (°C)	5 (0)	5 (10)	Wang et al., (2022a)
CN2a	SCS runoff curve number for soil hydrologic group A	21	35	Wang et al., (2022a)
CN2b	SCS runoff curve number for soil hydrologic group B	46	54	Wang et al., (2022a)
CN2c	SCS runoff curve number for soil hydrologic group C	59	64	Wang et al., (2022a)
CN2d	SCS runoff curve number for soil hydrologic group D	65	69	Wang et al., (2022a)
BLAI	Maximum leaf area index	6.02 ± 0.2	5.70 ± 0.2	MODIS
DLAI	Leaf area index when dormancy starts	0.86 (0.99)	0.71 (0.99)	MODIS
BIO_E	Radiation use efficiency	17 (15)	28.2 (15)	(Yang and Zhang, 2016)
BIO_LEAF	Leaf to biomass fraction	0.02 (0.3)	0.033 (0.3)	(Yang and Zhang, 2016)
EXT_COEF	Light extinction coefficient	0.41 (0.65)	0.46 (0.65)	Melnikova et al., (2018)

*Abbreviations: Leaf area index (LAI); Soil Conservation Service (SCS); Moderate-resolution imaging spectroradiometer (MODIS).

of forest growth on GWR and ET and differentiate the impacts of climate change from those of forest growth on the hydrological processes. In the *Forest Growth Scenario (FGS),* the focus was placed on the influence of forest development by analyzing the annual LAI trends of the FOEN species, which has dominated the landscape for several decades following its establishment in the mid-1950s. Default parameters were maintained for all other land use classes. In the *Climate Change Scenario (CCS),* climate conditions from the mid-1950s to the mid-1970s were applied to land use conditions representative of the 2000s to the 2010s. This configuration ensured that any observed changes in GWR and ET could be attributed exclusively to climate variability and change.

2.5. Model implementation, calibration, and validation

The Asahi River Catchment model was developed using the SWAT 2012 software (version 681) (Arnold et al., 1998), with input data summarized in Table 2. A 30-meter DEM was used to delineate the

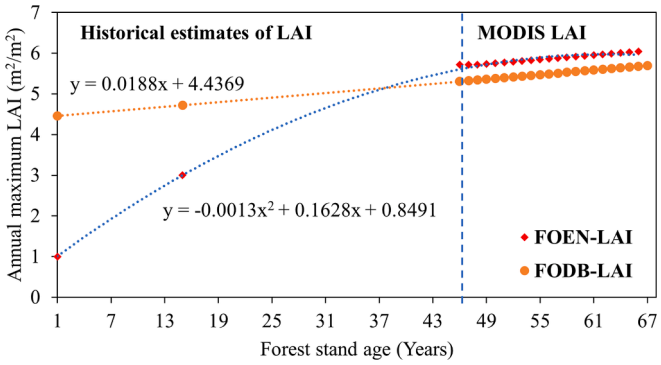

Fig. 2. Estimated historical annual maximum LAI derived from published literature and MODIS LAI products. The red diamonds and orange circles represent the annual maximum LAI for evergreen coniferous (FOEN-LAI) and deciduous broadleaf (FODB-LAI), respectively.

catchment and divide it into 32 subbasins, which were further disaggregated into several hydrologic response units (HRUs) based on land use, soil, and slope characteristics. At the HRU level, the hydrological responses of specific land covers, such as forest species, were simulated at a field scale, allowing their impacts on hydrological fluxes to be upscaled to subbasins and the entire catchment (Neitsch et al., 2011). The model setup reflected land use conditions from the 2000s to the 2010s, integrating data from the Ministry of Land, Infrastructure, Transport and Tourism (MLIT) and the Japan Aerospace Exploration Agency (JAXA) (Table 2). Forest growth for each species was represented by the annual change in LAI and extended back to 1955, as discussed in Section 2.3. Since land use changes in forested areas are minimal (Rendilicha et al., 2024), forest conversions were not considered. Soil classes were extracted from the MLIT database, and soil physical properties were obtained from the Harmonized World Soil Database (HWSD, version 2.0) (FAO, 2023) (Table 2).

The model was run to simulate both "present" and "historical" periods using daily weather forcing data covering 71 years, including a 5-year warm-up period. The "present" period was divided into a calibration phase from 2002 to 2011 and a validation phase from 2012 to 2021. Using the automated SWAT-CUP program (Abbaspour et al., 2007), the parameters for plant growth and hydrology were adjusted to match the SWAT-simulated LAI, ET, and streamflow with the smoothed MODIS-derived LAI, PML_V2 ET, and the observed streamflow data, respectively. Calibration began with parameters controlling LAI development at the HRU level, ensuring that the simulated minimum and maximum LAI values aligned with the MODIS LAI product (Haas et al., 2022a; Wang et al. 2022a).

Subsequently, ET and streamflow were calibrated. ET, especially for the FODB and FOEN forest species, was calibrated at the HRU level and further refined in three subbasins (shaded area in Fig. 1a) using PML_V2 ET data. At the subbasin level, PML_V2 ET estimates were derived from broader subbasin boundaries that included multiple land use categories to improve the overall accuracy of catchment-scale water balance estimation. Streamflow calibration was performed at two hydrological stations: Kanagawa and Makiyama (Fig. 1). This approach facilitated a robust multi-site and multi-variable calibration, which is critical for improving the estimation of hydrological budget components (Luo et al., 2023). Due to the lack of observed biomass data, the calibration prioritized LAI, with the assumption that accurate simulation of LAI, together with biomass and ET parameters, would sufficiently capture the dynamics of the water balance.

The "historical" period (1955–1999) was simulated at 5-year intervals. In the absence of observed data for the earlier years, the calibrated and validated parameters from the "present" period were applied to investigate the impacts of forest growth on GWR and ET from planting through maturity. Estimated historical annual maximum LAI values

Table 2
Details of the data used for simulation, along with relevant characteristics and data sources.

	Data	Description	Data source
Model input data	Topography	DEM (resolution of 30 m)	Advanced Spaceborne Thermal Emission and Reflection Radiometer (ASTER) (NASA, 2024)
	Land use and cover	Multi-source land use data	Japan Aerospace Exploration Agency (JAXA) and Ministry of Land, Infrastructure, Transport and Tourism (MLIT)
	Soil	Soil shapefile and physical properties	MLIT and Harmonized World Soil Database (HWSD version 2.0) (FAO, 2023)
	Climate	Daily precipitation, temperature, solar radiation, wind speed, humidity	Japan Meteorological Agency (JMA)
	Reservoirs	Reservoir specifications and daily outflows	Okayama Prefecture, dam databases
Model calibration	LAI	4-day composited dataset at 500-m resolution	Moderate resolution imaging spectroradiometer (MODIS) (AppEEARS, 2024)
	Streamflow	Daily river discharge (m3/s)	Water Information System (WIS), MLIT
	ET	8th day dataset of ET components at 500-m resolution	Penman–Monteith–Leuning Evapotranspiration V2 (PML_V2) products (Zhang et al., 2019)

*Abbreviations: Leaf area index (LAI), Evapotranspiration (ET), Digital elevation model (DEM).

(Fig. 2) were averaged at 5-year intervals and updated in the model. Model performance was evaluated using three standard statistical indices: coefficient of determination (R^2), Nash–Sutcliffe Efficiency (NSE), and percentage of bias (PBIAS) (Nash & Sutcliffe, 1970; Moriasi et al., 2015).

3. Results

3.1. Model performance evaluation

Model performance for the "present" period was evaluated using three target variables, LAI, ET, and streamflow,at both the HRU and subbasin scales. The simulated seasonal leaf development curves for FOEN (Fig. 3a) and FODB (Fig. 3b) closely aligned with those derived from MODIS LAI observations. A consistent annual increase in LAI was observed from 2002 to 2021, with a growth rate of 0.02 per year. The model effectively captured the onset and end of the growing season, with peak LAI values occurring between June and September, in agreement with field-based observations. Model performance was classified as "very good" during the calibration phase and "good" during the validation phase, as indicated by the R^2, NSE, and PBIAS metrics (Table 3). These results suggest a strong model's ability to represent both seasonal and inter-annual forest growth dynamics. However, a noticeable time lag was observed in the SWAT-simulated LAI values, which is likely attributable to the use of uncalibrated biomass parameters (e.g., BMX_TREES, MAT_YRS) that govern long-term forest growth and LAI development.

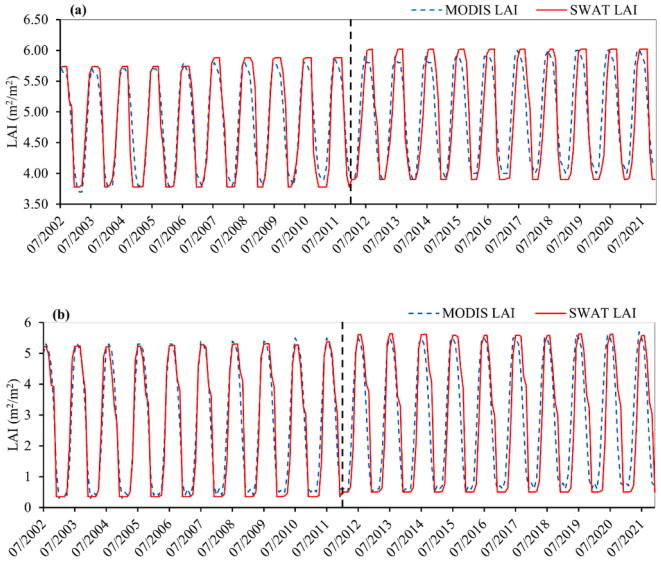

Fig. 3. Fitted MODIS LAI and SWAT LAI growth curves for (a) evergreen coniferous (FOEN) and (b) deciduous broadleaf (FODB) forests at the hydrologic response unit (HRU) level.

Table 3
SWAT model performance for predicting monthly LAI, ET and streamflow.

Calibration (Validation)	Targets	R^2	NSE	PBIAS
LAI HRU-scale	FODB	0.93 (0.73)	0.92 (0.67)	1.2 (−0.8)
	FOEN	0.91 (0.76)	0.88 (0.69)	0.1 (1.3)
Streamflow Channel	Kanagawa station	0.90 (0.79)	0.82 (0.78)	9.6(3.6)
	Makiyama station	0.91 (0.81)	0.82 (0.80)	13.8 (5.0)
Evapotranspiration HRU-scale	FODB	0.73 (0.79)	0.73 (0.76)	4.5 (10.7)
	FOEN	0.83 (0.83)	0.75 (0.77)	−0.28 (14.4)
Evapotranspiration Subbasin-scale	Subbasin 4	0.78 (0.88)	0.77 (0.86)	0.6 (−5.0)
	Subbasin 5	0.80 (0.88)	0.77 (0.84)	−3.1 (−8.3)
	Subbasin 22	0.82 (0.89)	0.81 (0.89)	5.9 (2.2)

*Abbreviations: Leaf area index (LAI), Hydrologic response unit (HRU), Deciduous broadleaf forest (FODB), Evergreen coniferous forest (FOEN), Nash–Sutcliffe efficiency (NSE), Percentage of bias (PBIAS), Coefficient of determination (R^2).

The model simulated the annual and seasonal variability of ET very well at both the HRU (Fig. 4a, b) and subbasins (Fig. 5a, b, c) levels, with the R^2, NSE, and PBIAS values meeting the "very good" criteria assuming the standards established for streamflow by Moriasi et al. (2015) (Table 3). The calibration and validation performance at the subbasins level were better than those at the HRU level, owing to the nature of finer spatial scale and species differentiations at the HRU level which introduces more variability and magnifying potential errors. Moreover, the SWAT model showed an underestimation of ET for FOEN during validation and also underestimated ET overall for FODB, which could be linked to uncertainties in both the satellite remote sensing methods represented by PML_V2 and SWAT approach (Zhang et al., 2019; Wang et al., 2022a).

The simulated streamflow during the calibration and validation periods correspond well with the observed flows at the Kanagawa and Makiyama stations (Fig. 6a, b). The performance indicators (R^2 and NSE) depicted "good" and "very good" criteria (Table 3). However, peak values were underestimated, particularly at the Makiyama station (PBIAS of about 13.8 %). This underestimation of peak flows is attributed to reservoir releases conducted before the flooding season to control the water levels in anticipation of high rainfall and extreme flows. The SWAT model poses limitations in accurately accounting for these operational interventions, interrupting standard flow patterns (Rendilicha et al., 2024).

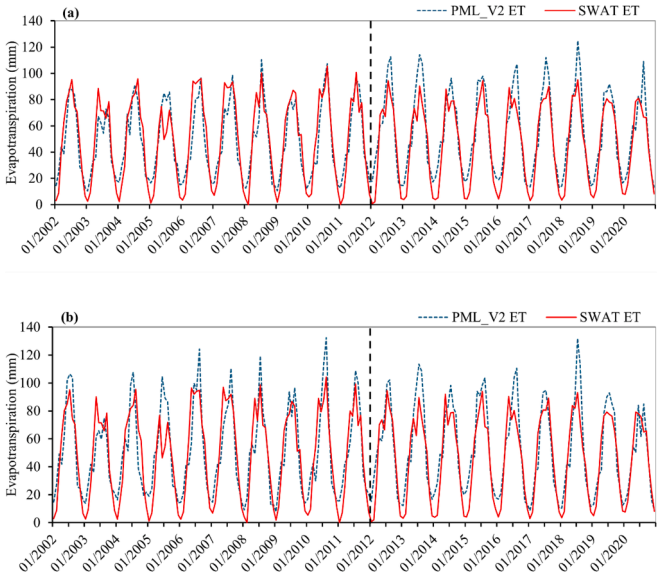

Fig. 4. Comparison of remote sensing-based PML_V2 ET and SWAT ET for (a) evergreen coniferous (FOEN) and (b) deciduous broadleaf (FODB) at hydrologic response unit (HRU) level.

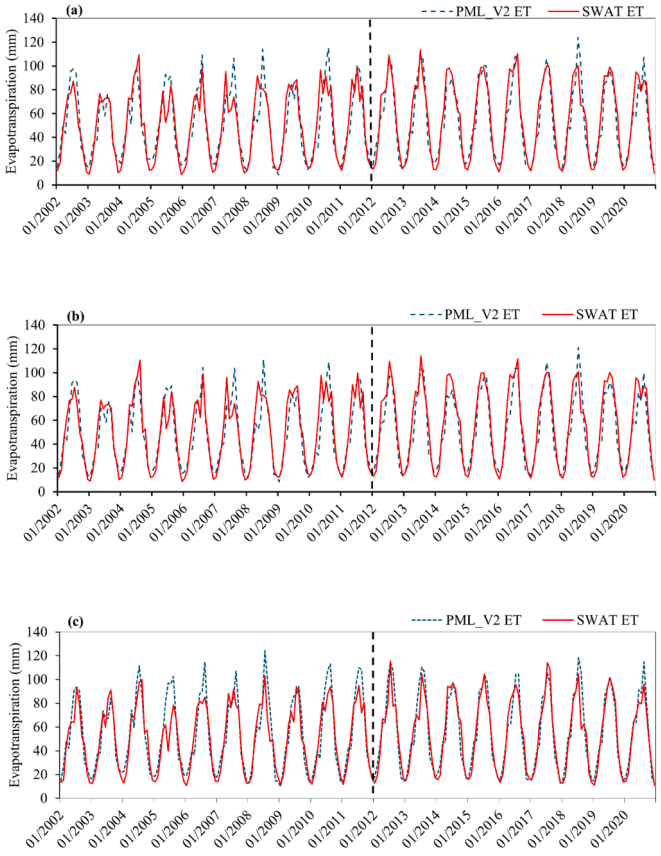

Fig. 5. Comparison of remote sensing-based PML_V2 ET and SWAT ET at (a) Subbasin 4, (b) Subbasin 9, and (c) Subbasin 22.

3.2. Scenario 1: Forest growth scenario (FGS)

The calibrated SWAT model was applied to simulate the impact of FODB and FOEN on the hydrological fluxes for 1955–2021. The FOEN was of particular interest, as they were transplanted in the catchment

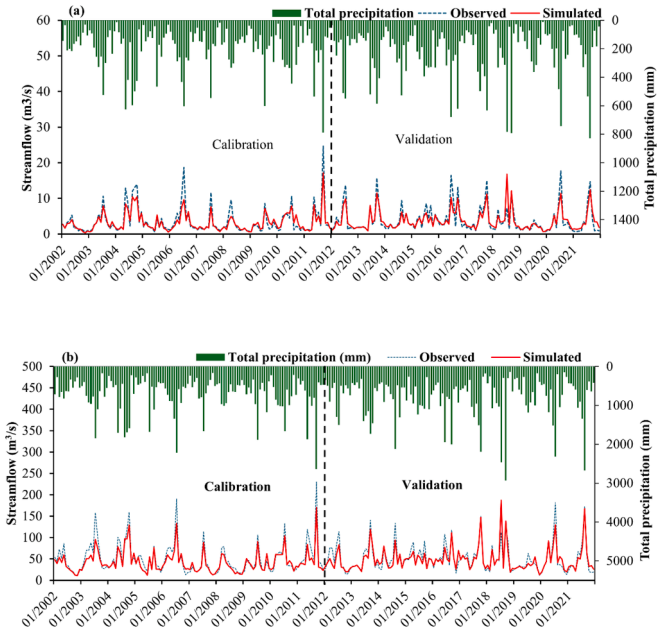

Fig. 6. Comparison of the streamflow and precipitation estimated using the soil and water assessment tool (SWAT) model and the data observed at the (a) Kanagawa and (b) Makiyama (b) gauge stations.

area around 1955 and have since matured. The FODB contained natural, old and matured forests (at the start of the simulation), serving as a baseline for comparison. Fig. 7a presents the annual water budget of surface runoff (SURQ), GWR, and ET for the FOEN category, depicting a clear trend of increasing ET and decreasing GWR over the initial 20 years of the simulation period, during which annual precipitation remained relatively constant. This indicates that as the FOEN matured, it consumed more water through ET, resulting in reduced GWR. In contrast, the mature FODB (Fig. 7b) displayed stable trends with respect to ET and GWR (during the same period), suggesting that the mature

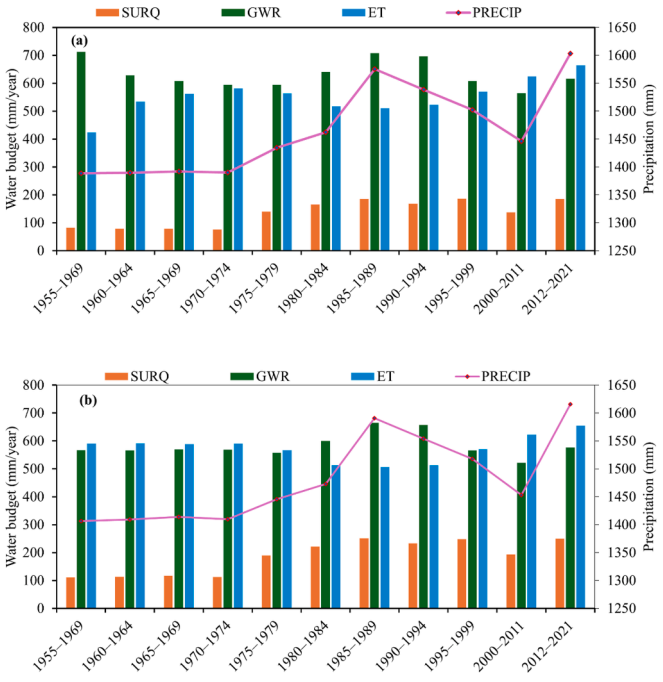

Fig. 7. Five-year annual average water budget during the growth stages of (a) FOEN and (b) FODB.

trees had stable water consumption compared to growing trees due to their established systems.

Fig. 8 illustrates the broader implications of afforestation of FOEN for the entire catchment area since 1955, revealing the potentially significant impacts of large afforestation programs on the hydrological fluxes within the catchment. Following the initiation of afforestation in 1955, an upward trend in ET was observed, reflecting increased water transpiration by maturing trees, consistent with forest maturation dynamics. In parallel, a declining trend in GWR was noted, indicating increased water uptake for ET, which led to reduced groundwater replenishment.

After reaching maturity, a decline in ET and an increase in GWR were observed, despite rising precipitation levels. However, as the forest continued to age (mid-1980s onward), ET increased, and GWR decreased. It is important to note that surface runoff (SURQ) and lateral flow (LATQ) remained stable, varying primarily in response to changes in precipitation.

3.3. Scenario 2: Climate change scenario (CCS)

Table 4 presents a comparison of hydrological results under different weather conditions. The "Actual" results for 1955–1974 reflect the historical climate and land use conditions, while the "Actual" results for 2002–2021 represent actual climate conditions, serving as a baseline for analyzing the CCS. The "CCS" results for 2002–2021 show the scenario results which excluded climate change impact. Observed climate data from the mid-1950s to 2010s indicate a clear warming trend, with a temperature increase of about 0.5 °C and a reduction in precipitation of 20 mm/year, consistent with the findings of Schaefer and Domroes (2009). Across the study area, the CCS resulted in a 25 % decrease in GWR compared to the actual conditions during the period from 2002 to 2021, while ET showed a modest net change of 6 %. For specific vegetation types, differentiated responses were observed. In areas dominated by FOEN species, GWR decreased by 22 %, with a corresponding ET increase of 7 %. Similarly, for FODB species, GWR decreased by 21 %, with an ET increase of 6 %. These results suggest that different vegetation types (FOEN and FODB) respond slightly differently to changes in climate conditions. The decline in GWR is more substantial than the decrease in ET highlighting the compounded effect of climate change (warming) and increased ET (as a result of forest growth) on GWR.

4. Discussion

4.1. Model evaluation

Model evaluation is key to enhancing the usefulness of model predictions (Sánchez-Dávila et al., 2023), thereby supporting informed decision-making. In this study, SWAT was developed to integrate multiple data sources for simulating the impacts of forest growth and climate change on the hydrological processes across large

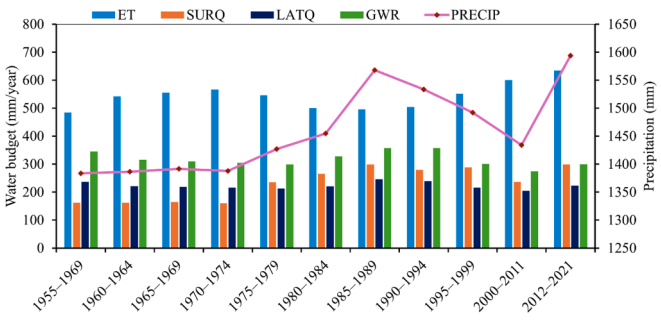

Fig. 8. Overall catchment water balance over 67 years (Five-year annual average), showing an initial upward trend in ET following the afforestation of FOEN in the mid-1950s, a subsequent decline after forest maturity, and another upward trend after the 1980s.

Table 4
Changes in average annual GWR and ET under the climate change scenario between two periods (1955–1974 and 2002–2021).

Variable	Actual GWR (1955–1974)	CCS GWR (2002–2021)	Actual GWR (2002–2021)	Difference (%)
Study area	506	504	404	−25 %
FOEN	617	606	497	−22 %
FODB	599	598	496	−21 %
	Actual ET (1955–1974)	CCS ET (2002–2021)	Actual ET (2002–2021)	
Study area	586	596	635	+6 %
FOEN	606	624	669	+7 %
FODB	620	622	662	+6 %

spatiotemporal scales. The model incorporates numerous parameters to capture dynamic processes and their nonlinear interactions, capabilities that exceed those of simple conceptual models, but this complexity also introduces greater uncertainty, necessitating careful calibration and validation to ensure reliable results. LAI, a key indicator of forest density and growth, directly influences hydrological components such as canopy evaporation, transpiration, and soil evaporation, making its accurate simulation essential for reliable prediction of evapotranspiration and overall water balance dynamics (Haas et al., 2022a). The SWAT-predicted intra- and inter-annual LAI dynamics matched well with MODIS-derived LAI datasets (Fig. 3a, b), and the model's statistical performance surpassed that of Haas et al. (2022a), even though both studies used the standard SWAT model without source code modifications. Between 2002 and 2021, the observed BLAI values increased from 5.72 to 6.02 m^2/m^2 for the FOEN species and from 5.34 to 5.70 m^2/m^2 for the FODB group, corresponding to annual growth rates of 0.018/year and 0.023/year, respectively. The seasonal LAI growth and inter-annual variations noted in this study agreed with those reported in previous studies, as discussed below.

Nasahara et al. (2008) estimated the LAI at the field scale in the canopy of the FODB group near Takayama in central Japan; the seasonal LAI growth began in May, peaking between June and the end of September, with the maximum LAI being 5 m^2/m^2, similar to our findings. Melnikova et al. (2018) estimated the LAI for the mountain forests of central Japan using the Landsat Operational Land Imager imagery (spatial resolution of 30 m), noting maximum LAI values of 5.5 ± 0.2 and 5.3 ± 0.2 m^2/m^2 for FODB and FOEN, respectively. The average values calculated in this study were within these ranges despite the difference in the spatial resolution. Wang et al. (2022a) fitted the LAI values for the Yamato River catchment using an improved version of the SWAT model (SWAT-T); their estimates of the BLAI values for both the forest species were close to those estimated in this study. Sumida et al. (2018) analyzed the inter-annual variability of LAI for an evergreen conifer stand over 19 years, using allometric methods, with the LAI values varying between 7.1 and 8.8 m^2/m^2, which were higher than those reported in this study. The higher LAI estimates obtained using allometric methods, compared with the LAI estimates obtained using MODIS data, is due to mismatch in scales between the two datasets (Wang et al., 2017). Additionally, Ma et al. (2023) reported a significant increase in LAI across different vegetation types in China between 2001 and 2021, with an overall inter-annual growth rate of 0.0202/year, which closely aligns with the growth rate estimates in our study.

Fig. 9 presents the 5-year annual average long-term LAI development curves simulated using the SWAT model for 1955–1921, based on the calibrated parameters. The SWAT model clearly captured the distinction between the inter-annual growth in the LAIs of natural, old and mature FODB and FOEN forests planted in the mid-1950s. In a study by Nasahara et al. (2008) and as discussed by Potithep et al. (2010), the FODB forest LAIs measured in-situ in 2005 and 2006 were 0.5 and 5 m^2/m^2,

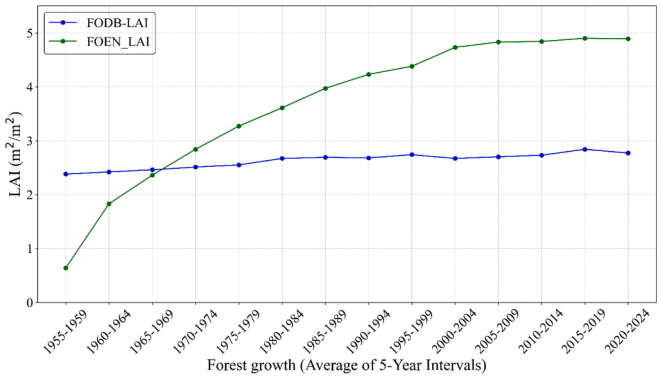

Fig. 9. Five-year annual average of historical forest Leaf Area Index (LAI) as simulated by the SWAT model for the period 1955–2021.

respectively; the average of these values agrees with the average value noted in this study. Differing from deciduous trees, which renew all their leaves every year, evergreen conifers shed only part of their needle leaves in the fall and grow a similar amount in the spring (Wang et al., 2017). Thus, for growing evergreen conifers, more leaves are added in the subsequent years, and the annual average continues to grow.

While the proposed model demonstrated effectiveness, critical considerations for applying the standard SWAT model in forest water balance estimation must be acknowledged. Hydrological models generally face three types of uncertainties/limitations: structural, application-related, and input-related (Wagener et al., 2001). Some structural limitations can be addressed through model application or methodological adjustments. In this study, the structural limitations regarding static BLAI and ALAI_MIN, as well as potential misrepresentation of seasonal forest growth, were addressed by using short-term simulation intervals and removing management settings from the model. Notably, this approach did not require any modifications to the SWAT source code, as such changes would have increased model complexity and necessitated additional files and parameters, potentially hindering the model's applicability (Haas et al., 2024).

The model's uncertainties arise from the assumptions made during the reconstruction of historical forest growth and climate data. In this study, historical forest development was inferred using remote sensing-derived LAI data from the 2000s and 2010s, combined with data from previous studies. The 5-year annual average LAI, spanning 67 years, was estimated through a simple interpolation technique, which introduced uncertainty into the modeling process. The undergrowth, likely established during the transplantation of the FOEN species or developed over time, was not included in the model due to the complexity of representing ecosystem diversity, which further contributed to model uncertainty. Additionally, climate data for the 1950s to 1970s were limited to only one station, with the remaining data simulated by the SWAT model's weather generator (WGEN). The reliance on a single station and the limitations of the simulated data further contributed to model uncertainty, particularly in accurately representing historical climate variability and its impact on hydrological fluxes in the region. However, in the absence of comprehensive historical data, the current approach is deemed sufficient for informing forest management strategies, as it offers a pragmatic balance between data availability and model reliability.

4.2. *Impact of forest growth and climate change*

Forest regeneration and expansion are recognized as nature-based solutions to address climate change and promote sustainable development (Sun et al., 2023). Understanding the dynamics of hydrological fluxes immediately after forest establishment is crucial, particularly within the context of Japan, because 60 % of man-made forests in the country are privately owned, and forest practices (such as planting, thinning, and harvesting) are often conducted intermittently for economic purposes (Sakai, 1999). With the rotation age in man-made forests planned to be 40 years (Hirata et al., 2006), frequent forest ecosystem disturbances are expected. This study contributes to understanding how catchment hydrology changes in the years following afforestation, which is essential for ensuring the sustainability of water resources and afforestation programs (Bentley & Coomes, 2020).

Fig. 10 illustrates the dynamics of ET and the age of FOEN species during the first 20 years after forest establishment. The analysis of covariance (ANCOVA) model, which assessed the effect of forest growth on ET while controlling for precipitation, revealed a positive and statistically significant coefficient of 7.6 (p-value < 0.001). This indicates that as the forest matured, ET increased by approximately 7.6 mm/year, with precipitation remaining constant during this period. This finding is consistent with the consensus that forest establishment can lead to reduced river flow due to increased transpiration and interception rates (Bruijnzeel, 2004; Filoso et al., 2017).

A decrease in ET was observed in the initial period, followed by a marked increase, suggesting that young trees with smaller leaf area and lower transpiration rates dominated this phase. As the forest matured, increased LAI and higher transpiration rates contributed to the rise in ET. This is consistent with findings from California's Sierra Nevada, where post-disturbance forests exhibited lower ET due to reduced biomass and leaf area (Roche et al., 2020). The recurrent ET fluctuations observed in this study, unexplained by forest growth and precipitation, may be attributed to environmental factors such as wind patterns associated with the East Asian monsoon. These changes could have influenced evapotranspiration in the region through wind-driven mixing and heat exchange (Chen et al., 2023a; Nagano et al., 2023).

The variations in GWR caused by the growth of FOEN over a 20-year period (1955–1974) in a steep forested catchment in Japan is shown in Fig. 11. The ANCOVA model revealed a statistically significant negative coefficient of -4.7 (p-value < 0.0001), indicating that GWR in the region decreased by approximately 4.7 mm/year as the forests aged, while precipitation remained relatively constant during this period. The decrease in GWR was likely due to increased water uptake by the maturing forest, which reduced the water available for GWR. This conclusion is consistent with the observed increase in ET and aligns with previous studies indicating that forest systems generally exhibit lower GWR compared to other land uses due to their higher evapotranspiration rates (Owuor et al., 2016; Taniguchi et al., 1996). Hwang et al. (2023) further suggest that forest hydrology is significantly influenced by seasonal variations, particularly during transitions in leaf phenology, which impact soil moisture and streamflow dynamics.

The overall GWR estimated in this study was compared with that of Rendilicha et al. (2024) for the period 2009–2019 across the entire catchment, as the species-level comparison was not possible because Rendilicha et al. (2024) considered all the forest biomes in a single forest

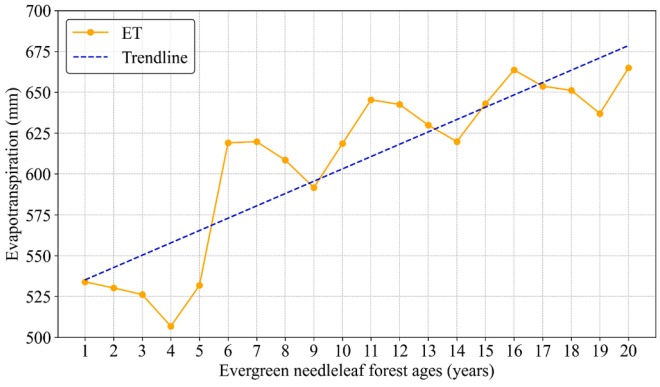

Fig. 10. Variations in the ET due to evergreen coniferous forest (FOEN) growth over a 20-year period.

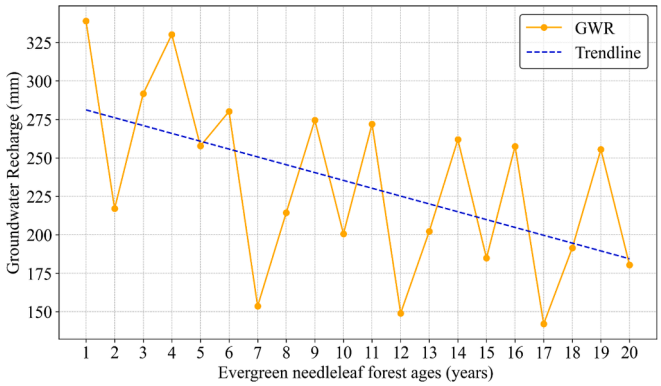

Fig. 11. Variations in GWR caused by the growth of evergreen coniferous forest (FOEN) over a 20-year period.

cover category. In the current study, the overall average annual GWR for 2009–2019 was estimated at 422 mm/year, which is lower than the 471 mm/year reported by Rendilicha et al. (2024). The PBIAS of the streamflow improved (underestimation) by almost half at both the Makiyama and Kanagawa stations. Similar improvements were reported in previous studies (Chen et al., 2023b; Haas et al., 2022a; b; Wang et al., 2022a), which demonstrated that improved forest growth representation and multi-calibration enhanced model's accuracy in simulating evapotranspiration, thereby reducing the previously overestimated or underestimated subsurface flows and surface runoff.

Furthermore, the overall predictions of ET and runoff in this study differed from those presented by Rendilicha et al. (2024), with ET showing a decreasing trend (from 682 mm/year to 635 mm/year) and runoff exhibited an increasing trend (from 189 mm/year to 299 mm/year) over the same period. Lateral flows remained similar in both studies. These discrepancies are likely due to the use of PML-V2 ET data in the current study, in contrast to ET estimates derived from traditional streamflow calibration in Rendilicha et al., (2024) and MODIS-derived ET data used in earlier studies. MODIS ET data is known to overestimate ET in some regions, whereas the PML-V2 ET model is recognized for providing more accurate results (Yuan et al., 2024; He et al., 2022; Gan et al., 2018). In this catchment, the prediction was based on observed streamflow analysis, with the mean daily discharge (1979–2021) at the Makiyama outlet being relatively high (~53.89 m^3/s), and the forested steep slopes being covered with a thin layer of cambisols, with moderate hydraulic conductivity.

Studies on hydrological fluxes related to climate change often rely on projected future climate conditions (Al Atawneh et al., 2021), using General Circulation Models (GCMs) or scenario analyses that adjust temperature and precipitation to create perturbed climate conditions (Condon et al., 2020). While these approaches help predict potential future changes, they may introduce errors or unrealistic outcomes compared to using observed historical climate data (Feng and Beighley, 2020) By relying on long-term historical climate data, this study reduces uncertainties inherent in climate models and future assumptions, providing a more reliable assessment of climate change impacts on hydrological processes.

The results from our CCS indicate a significant decline in GWR and a rise in ET, with the reduction in GWR being more pronounced than the increase in ET (Table 4). This could be explained by the increase in ET due to warming (rise in air temperature), which further reduces the potential for GWR, creating a compounding effect. Similarly, Condon et al. (2020), who studied the depletion of groundwater by ET under warming over the contiguous United States, found that increased evaporative demand due to warming leads to a decrease in groundwater storage, particularly in energy-limited regions where ET is not constrained by water supply. Similar decreases in GWR have been reported in other studies, such as Natkhin et al. (2012), who observed a reduction of about 40 mm/year in a catchment in Germany, and Al Atawneh et al. (2021), who documented decreasing GWR due to climate change. These studies highlight a common trend of reduced GWR and increased ET under changing climatic conditions, consistent with the findings of the current study.

5. Conclusions

This study analyzed and quantified the impacts of historical forest growth trends and climate change on hydrological fluxes,specifically GWR and ET,during the critical transition period from planting to maturity, a developmental stage that plays a key role in shaping catchment-scale water balance. Long-term forest growth trends, encompassing the complete ontogenetic continuum from juvenile to post-mature stages of a representative species, were reconstructed by integrating multiple data sources and incorporated into the SWAT model to simulate their hydrological consequences, with GWR and ET serving as proxies for forest ecosystem function and hydrological health. The growth of FOEN species significantly influenced the hydrological fluxes, particularly from the establishment phase to maturity. The GWR in the region decreased by approximately 4.7 mm/year, while ET increased by 7.6 mm/year from 1955 to 2021. In contrast, the mature, naturally occurring FODB category exhibited more stable trends concerning both GWR and ET. Among the climate variables, rising temperatures were the cause of decreased groundwater recharge and increased evapotranspiration, reflecting the impact of global warming as observed in recent decades. The dynamics of forest growth and their interaction with climate change play a crucial role in regulating the water balance of forested catchments, particularly during the developmental stage and especially in regions with transitional forest ecosystems. Incorporating these dynamics into water resource planning is therefore essential to sustaining groundwater recharge and promoting effective groundwater conservation efforts. This study also demonstrates that integrating hydrological modeling with remote sensing, historical forest inventories, and previous field-scale studies offers a robust approach for analyzing long-term hydrological processes during periods of data scarcity.

Funding source

This research was supported by JSPS Grant-in-Aid for Scientific Research (B) (No. 21H03650, PI: Mitsuyo Saito), Fostering Joint International Research (A) (No. 20KK0262, PI: Mitsuyo Saito), and the Asia-Pacific Network for Global Change Research (APN) under Grant No. CRRP2019-09MY-Onodera (funder ID: http://dx.doi.org/10.13039/100005536).

CRediT authorship contribution statement

Rendilicha Halake Guyo: Conceptualization, Data curation, Formal analysis, Investigation, Methodology, Software, Validation, Visualization, Writing – original draft, Writing – review & editing. **Kunyang Wang:** Writing – review & editing, Supervision, Methodology, Conceptualization. **Shin-ichi Onodera:** Supervision, Resources, Funding acquisition, Conceptualization. **Mitsuyo Saito:** Writing – review & editing, Supervision, Resources, Conceptualization. **Toshitsugu Moroizumi:** Supervision.

Declaration of competing interest

The authors declare that they have no known competing financial interests or personal relationships that could have appeared to influence the work reported in this paper.

Acknowledgment

We are grateful to the Asahi River Dam Integrated Management Office for providing daily discharge data from the dams.

Data availability

Data supporting study findings available from corresponding author upon request.

References

Abbaspour, K.C., Vejdani, M., Haghighat, S., Yang, J. (2007, December). SWAT-CUP calibration and uncertainty programs for SWAT. In MODSIM 2007 international congress on modelling and simulation, modelling and simulation society of Australia and New Zealand (pp. 1596-1602). Dübendorf, Switzerland: Swiss Federal Institute of Aquatic Science and Technology.

Aber, J.D., Nadelhoffer, K.J., Steudler, P., Melillo, J.M., 1989. Nitrogen saturation in northern forest ecosystems. Bioscience 39 (6), 378. http://www.jstor.org/stable/1311067?origin=JSTOR-pdf.

AppEEARS: Application for Extracting and Exploring Analysis Ready Samples of NASA, available at https://appeears.earthdatacloud.nasa.gov/ (last access 5 August 2024), 2024.

Al Atawneh, D., Cartwright, N., Bertone, E., 2021. Climate change and its impact on the projected values of groundwater recharge: a review. J. Hydrol. 601, 126602. https://doi.org/10.1016/j.jhydrol.2021.126602.

Arnold, J.G., Srinivasan, R., Muttiah, R.S., Williams, J.R., 1998. Large area hydrologic modeling and assessment part i: model development. JAWRA J. Am. Water Resour. Assoc. 34 (1), 73–89. https://doi.org/10.1111/j.1752-1688.1998.tb05961.x.

Bentley, L., Coomes, D.A., 2020. Partial river flow recovery with forest age is rare in the decades following establishment. Glob. Chang. Biol. 26 (3), 1458–1473. https://doi.org/10.1111/gcb.14954.

Bosch, J.M., Hewlett, J.D., 1982. A review of catchment experiments to determine the effect of vegetation changes on water yield and evapotranspiration. J. Hydrol. 55 (1–4), 3–23. https://doi.org/10.1016/0022-1694(82)90117-2.

Brown, A.E., Zhang, L., McMahon, T.A., Western, A.W., Vertessy, R.A., 2005. A review of paired catchment studies for determining changes in water yield resulting from alterations in vegetation. J. Hydrol. 310 (1–4), 28–61. https://doi.org/10.1016/j.jhydrol.2004.12.010.

Bruijnzeel, L.A., 2004. Hydrological functions of tropical forests: not seeing the soil for the trees? Agric. Ecosyst. Environ. 104 (1), 185–228. https://doi.org/10.1016/j.agee.2004.01.015.

Chen, P., Ma, J., Ma, X., Yu, Q., Cui, X., Guo, J., 2023a. Groundwater recharge in typical geomorphic landscapes and different land use types on the loess plateau, China. Hydrol. Process. 37 (4). https://doi.org/10.1002/hyp.14860.

Chen, S., Fu, Y.H., Wu, Z., Hao, F., Hao, Z., Guo, Y., Geng, X., Li, X., Zhang, X., Tang, J., Singh, V.P., Zhang, X., 2023b. Informing the SWAT model with remote sensing detected vegetation phenology for improved modeling of ecohydrological processes. J. Hydrol. 616. https://doi.org/10.1016/j.jhydrol.2022.128817.

Condon, L.E., Atchley, A.L., Maxwell, R.M., 2020. Evapotranspiration depletes groundwater under warming over the contiguous United States. Nat. Commun. 11 (1), 873. https://doi.org/10.1038/s41467-020-14688-0.

Cuthbert, M.O., Gleeson, T., Moosdorf, N., Befus, K.M., Schneider, A., Hartmann, J., Lehner, B. (2019). Global patterns and dynamics of climate–groundwater interactions. In Nature Climate Change (Vol. 9, Issue 2, pp. 137–141). Nature Publishing Group. doi: 10.1038/s41558-018-0386-4.

de Vries, J.J., Simmers, I., 2002. Groundwater recharge: An overview of process and challenges. Hydrgeol. J. 10 (1), 5–17. https://doi.org/10.1007/s10040-001-0171-7.

FAO. Harmonized World Soil Database version 2.0. FAO and IIASA. Rome and Laxenburg. https://doi.org/10.4060/cc3823en.

Fassnacht, F.E., White, J.C., Wulder, M.A., Næsset, E., 2024. Remote sensing in forestry: current challenges, considerations and directions. Forestry 97 (1), 11–37. https://doi.org/10.1093/forestry/cpad024.

Feng, D., Beighley, E., 2020. Identifying uncertainties in hydrologic fluxes and seasonality from hydrologic model components for climate change impact assessments. Hydrol. Earth Syst. Sci. 24 (5), 2253–2267. https://doi.org/10.5194/hess-24-2253-2020.

Filoso, S., Bezerra, M.O., Weiss, K.C.B., Palmer, M.A., 2017. Impacts of forest restoration on water yield: a systematic review. PLoS One 12 (8), e0183210. https://doi.org/10.1371/journal.pone.0183210.

Flerchinger, G.N., Hanson, C.L., Wight, J.R., 1996. Modeling evapotranspiration and surface energy budgets across a watershed. Water Resour. Res. 32 (8), 2539–2548. https://doi.org/10.1029/96WR01240.

Gan, R., Zhang, Y., Shi, H., Yang, Y., Eamus, D., Cheng, L., Yu, Q., 2018. Use of satellite leaf area index estimating evapotranspiration and gross assimilation for Australian ecosystems. Ecohydrology 11 (5), e1974.

Goeking, S.A., Tarboton, D.G., 2020. Forests and water yield: a synthesis of disturbance effects on streamflow and snowpack in western coniferous forests. J. For. 118 (2), 172–192. https://doi.org/10.1093/jofore/fvz069.

Golden, H.E., Evenson, G.R., Tian, S., Amatya, D.M., Sun, G. (2016). Hydrological modelling in forested systems. Wallingford UK: CABI. doi: 10.1079/9781780646602.0141.

Haas, H., Reaver, N.G., Karki, R., Kalin, L., Srivastava, P., Kaplan, D.A., Gonzalez-Benecke, C., 2022a. Improving the representation of forests in hydrological models. Sci. Total Environ. 812, 151425. https://doi.org/10.1016/j.scitotenv.2021.151425.

Haas, H., Kalin, L., Srivastava, P., 2022b. Improved forest dynamics leads to better hydrological predictions in watershed modeling. Sci. Total Environ. 821, 153180. https://doi.org/10.1016/j.scitotenv.2022.153180.

Haas, H., Kalin, L., Yen, H., 2024. Improved forest canopy evaporation leads to better predictions of ecohydrological processes. Ecol. Model. 489 (December 2023), 110620. https://doi.org/10.1016/j.ecolmodel.2024.110620.

Haydon, S.R., Benyon, R.G., Lewis, R., 1997. Variation in sapwood area and throughfall with forest age in mountain ash (Eucalyptus regnans F. Muell.). J. Hydrol. 187 (3–4), 351–366.

He, S., Zhang, Y., Ma, N., Tian, J., Kong, D., Liu, C., 2022. A daily and 500m coupled evapotranspiration and gross primary production product across China during 2000-2020. Earth Syst. Sci. Data 14 (12), 5463–5488. https://doi.org/10.5194/essd-14-5463-2022.

Hirata, Y., Matsumoto, M., Iehara, T., 2006. Japanese national forest inventory and its spatial extension by remote sensing. In: Proceedings of the Eighth Annual Forest Inventory and Analysis Symposium, pp. 16–19.

Hou, X., Yang, H., Cao, J., Feng, W., Zhang, Y., 2023. A Review of advances in groundwater evapotranspiration research. Water 15 (5), 969. https://doi.org/10.3390/w15050969.

Hwang, T., Band, L.E., Oishi, A.C., Kang, H., 2023. Greenup variability impact on seasonal streamflow and soil moisture dynamics in humid, temperate forests. Water Resour. Res. 59 (12), 1–17. https://doi.org/10.1029/2022WR034125.

Ishii, T., Nashimoto, M., Shimogaki, H., 1999. Estimation of leaf area index using remote sensing data. J. Jpn Soc. Hydrol. Water Resour. 12 (3), 210–220. https://doi.org/10.3178/jjshwr.12.210.

Jasechko, S., Sharp, Z.D., Gibson, J.J., Birks, S.J., Yi, Y., Fawcett, P.J., 2013. Terrestrial water fluxes dominated by transpiration. Nature 496 (7445), 347–350. https://doi.org/10.1038/nature11983.

Kimbi, S.B., Onodera, S.I., Wang, K., Kaihotsu, I., Shimizu, Y., 2024. Assessing the impact of urbanization and climate change on hydrological processes in a suburban catchment. *Environments* 11 (10), 225. https://doi.org/10.3390/environments11100225.

Koirala, S., Yeh, P.-J.-F., Hirabayashi, Y., Kanae, S., Oki, T., 2014. Global-scale land surface hydrologic modeling with the representation of water table dynamics. J. Geophys. Res. Atmos. 119 (1), 75–89. https://doi.org/10.1002/2013JD020398.

Kuang, X., Liu, J., Scanlon, B.R., Jiao, J.J., Jasechko, S., Lancia, M., Zheng, C., 2024. The changing nature of groundwater in the global water cycle. Science 383 (6686), eadf0630. https://doi.org/10.1126/science.adf0630.

Kumar, C.P., 2012. Climate change and its influence on groundwater resources. International Journal of. Eng. Sci. 1 (5), 43–60.

Liu, Z., Cheng, L., Zhou, G., Chen, X., Lin, K., Zhang, W., Zhou, P., 2020. Global response of evapotranspiration ratio to climate conditions and watershed characteristics in a changing environment. J. Geophys. Res. Atmos. 125 (7), e2020JD032371. https://doi.org/10.1029/2020JD032371.

Luo, Z., Gao, Z., Wang, L., Wang, S., Wang, L., 2023. A method for balancing the terrestrial water budget and improving the estimation of individual budget components. Agric. For. Meteorol. 341 (December 2022), 109667. https://doi.org/10.1016/j.agrformet.2023.109667.

Ma, Y., Wang, W., Jin, S., Li, H., Liu, B., Gong, W., Fan, R., Li, H., 2023. Spatiotemporal variation of LAI in different vegetation types and its response to climate change in China from 2001 to 2020. Ecol. Ind. 156 (October), 111101. https://doi.org/10.1016/j.ecolind.2023.111101.

McShane, R.R., Driscoll, K.P., Sando, R., 2017. A review of surface energy balance models for estimating actual evapotranspiration with remote sensing at high spatiotemporal resolution over large extents. Sci. Invest. Rep. (2017-5087). https://doi.org/10.3133/sir20175087.

Melnikova, I., Awaya, Y., Saitoh, T., Muraoka, H., Sasai, T., 2018. Estimation of leaf area index in a mountain forest of central Japan with a 30-m spatial resolution based on Landsat operational land imager imagery: an application of a simple model for seasonal monitoring. Remote Sens. (Basel) 10 (2), 179. https://doi.org/10.3390/rs10020179.

Mensah, J.K., Ofosu, E.A., Yidana, S.M., Akpoti, K., Kabo-bah, A.T. (2022). Integrated modeling of hydrological processes and groundwater recharge based on land use land cover, and climate changes: A systematic review. In Environmental Advances (Vol. 8). Elsevier Ltd. doi: 10.1016/j.envadv.2022.100224.

Moriasi, D.N., Gitau, M.W., Pai, N., Daggupati, P., 2015. Hydrologic and water quality models: performance measures and evaluation criteria. Trans. ASABE 58 (6), 1763–1785. https://doi.org/10.13031/trans.58.10715.

Nagano, A., Kaneko, H., Wakita, M., 2023. Interannual sea-level variation around mainland Japan forced by subtropical North Pacific wind and its possible impact on the Tsugaru warm current. Ocean Dyn. 73 (12), 761–771. https://doi.org/10.1007/s10236-023-01580-w.

Nasahara, K.N., Muraoka, H., Nagai, S., Mikami, H., 2008. Vertical integration of leaf area index in a Japanese deciduous broad-leaved forest. Agric. For. Meteorol. 148 (6–7), 1136–1146. https://doi.org/10.1016/j.agrformet.2008.02.

Nang, Y.W., Onodera, S.-I., Wang, K., Shimizu, Y., Saito, M., 2024. Slope gradient effects on sediment yield of different land cover and soil types. Water 16 (1419). https://doi.org/10.3390/w16101419.

NASA: United States Geological Survey. Earth Explorer. Available at: http://earthexplorer.usgs.gov/ (Last accessed: 9 May 2024), 2014.

Nash, J.E., Sutcliffe, J.V., 1970. River flow forecasting through conceptual models part I, A discussion of principles. J. Hydrol. 10 (3), 282–290. https://doi.org/10.1016/0022-1694(70)90255-6.

Natkhin, M., Steidl, J., Dietrich, O., Dannowski, R., Lischeid, G., 2012. Differentiating between climate effects and forest growth dynamics effects on decreasing groundwater recharge in a lowland region in Northeast Germany. J. Hydrol. 448–449, 245–254. https://doi.org/10.1016/j.jhydrol.2012.05.005.

Neitsch, S.L., Arnold, J.G., Kiniry, J.R., Williams, J.R. (2011). Soil & Water Assessment Tool Theoretical Documentation Version 2009. Texas Water Resources Institute,

Technical Report No. 406. TR-406_SoilandWaterAssessmentToolTheoreticalDocumentation.pdf (tamu.edu).
Nita, M.D., Munteanu, C., Gutman, G., Abrudan, I.V., Radeloff, V.C., 2018. Widespread forest cutting in the aftermath of World War II captured by broad-scale historical Corona spy satellite photography. Remote Sens. Environ. 204, 322–332. https://doi.org/10.1016/j.rse.2017.10.021.
Okayama Prefecture Department of Agriculture, Forestry, and Fisheries, Forest Policy Division, Erosion Control Division, and Cooperative Guidance Division. (2021). Okayama Prefecture Forest and Forestry Statistics. Okayama Prefecture Department of Agriculture, Forestry, and Fisheries. https://www.pref.okayama.jp/soshiki/57/.
Owuor, S.O., Butterbach-Bahl, K., Guzha, A.C., Rufino, M.C., Pelster, D.E., Díaz-Pinés, E., Breuer, L., 2016. Groundwater recharge rates and surface runoff response to land use and land cover changes in semi-arid environments. Ecol. Process. 5 (1). https://doi.org/10.1186/s13717-016-0060-6.
Potithep, S., Nasahara, N.K., Muraoka, H., Nagai, S., Suzuki, R. (2010). What is the actual relationship between LAI and VI in a deciduous broadleaf forest. International Archives of the Photogrammetry, Remote Sensing and Spatial Information Science, 38(Part 8). W07F02_20100308114838.pdf (isprs.org).
Rendilicha, H.G., Wang, K., Saito, M., Onodera, S., Shimizu, Y., Moroizumi, T., 2024. Spatiotemporal shallow and deep groundwater dynamics in a forested mountain catchment with diverse slope gradients, western Japan. Groundw. Sustain. Dev. 25 (March), 101150. https://doi.org/10.1016/j.gsd.2024.101150.
Roche, J.W., Ma, Q., Rungee, J., Bales, R.C., 2020. Evapotranspiration mapping for forest management in California's Sierra Nevada. Front. For. Global Change 3. https://doi.org/10.3389/ffgc.2020.00069.
Sakai, M., 1999. Minds of forest owners for management and forest resources policy. J. For. Eco. 45, 3–8.
Sánchez-Dávila, J., De Cáceres, M., Vayreda, J., Retana, J., 2023. Regional patterns and drivers of water flows along environmental, functional and stand structure gradients in Spanish forests. Hydrol. Earth Syst. Sci. https://doi.org/10.5194/hess-2023-255.
Schaefer, D., Domroes, M., 2009. Recent climate change in Japan–spatial and temporal characteristics of trends of temperature. Clim. Past 5 (1), 13–19. https://doi.org/10.5194/cp-5-13-2009.
Shimizu, Y., Onodera, S.-I., Saito, M. (2011). Effect of climate change on nutrient discharge in a coastal area, western Japan (Vol. 348). IAHS Publ. http://meteocrop.dc.affrc.go.jp/.
Simic, A., Fernandes, R., Wang, S., 2014. Assessing the impact of leaf area index on evapotranspiration and groundwater recharge across a shallow water region for diverse land cover and soil properties. Int. Geosci. Remote Sens. Sympos. (IGARSS) 7, 4881–4884. https://doi.org/10.1109/igarss.2004.1370257.
Smettem, K.R.J., Waring, R.H., Callow, J.N., Wilson, M., Mu, Q., 2013. Satellite-derived estimates of forest leaf area index in southwest Western Australia are not tightly coupled to interannual variations in rainfall: implications for groundwater decline in a drying climate. Glob. Chang. Biol. 19 (8), 2401–2412. https://doi.org/10.1111/gcb.12223.
Sumida, A., Watanabe, T., Miyaura, T., 2018. Interannual variability of leaf area index of an evergreen conifer stand was affected by carry-over effects from recent climate conditions. Sci. Rep. 8 (1), 13590. https://doi.org/10.1038/s41598-018-31672-3.
Sun, G., Wei, X., Hao, L., Sanchis, M.G., Hou, Y., Yousefpour, R., Zhang, Z., 2023. Forest hydrology modeling tools for watershed management: a review. For. Ecol. Manage. 530, 120755. https://doi.org/10.1016/j.foreco.2022.120755.
Taniguchi, M., Tsujimura, M., Tanaka, T., 1996. Significance of stemflow in groundwater recharge. 1: evaluation of the stemflow contribution to recharge using a mass balance approach. Hydrol. Processes 10 (1), 71–80. https://doi.org/10.1002/(SICI)1099-1085(199601)10:1%3C71::AID-HYP301%3E3.0.CO;2-Q.
Verbesselt, J., Hyndman, R., Zeileis, A., Culvenor, D., 2010. Phenological change detection while accounting for abrupt and gradual trends in satellite image time series. Remote Sens. Environ. 114 (12), 2970–2980. https://doi.org/10.1016/j.rse.2010.08.003.
Wagener, T., Boyle, D.P., Lees, M.J., Wheater, H.S., Gupta, H.V., Sorooshian, S., 2001. A framework for development and application of hydrological models. Hydrol. Earth Syst. Sci. 5 (1), 13–26. https://doi.org/10.5194/hess-5-13-2001.
Wang, R., Chen, J.M., Liu, Z., Arain, A., 2017. Evaluation of seasonal variations of remotely sensed leaf area index over five evergreen coniferous forests. ISPRS J. Photogramm. Remote Sens. 130, 187–201. https://doi.org/10.1016/j.isprsjprs.2017.05.017.
Wang, K., Onodera, S., Saito, M., Shimizu, Y., 2021a. Long-term variations in water balance by increase in percent imperviousness of urban regions. *J. Hydrol.* 602 (January), 126767. https://doi.org/10.1016/j.jhydrol.2021.126767.
Wang, K., Onodera, S.I., Saito, M., Okuda, N., Okubo, T., 2021b. Estimation of phosphorus transport influenced by climate change in a rice paddy catchment using SWAT. *Int. J. Environ. Res.* 15 (4), 759–772. https://doi.org/10.1007/s41742-021-00350-0.
Wang, K., Onodera, S., Saito, M., Shimizu, Y., Iwata, T., 2022a. Effects of forest growth in different vegetation communities on forest catchment water balance. *Sci. Total Environ.* 809, 151159. https://doi.org/10.1016/j.scitotenv.2021.151159.
Wang, K., Onodera, S.I., Saito, M., 2022b. Evaluation of nitrogen loading in the last 80 years in an urbanized Asian coastal catchment through the reconstruction of severe contamination period. Environ. Res. Lett. 17 (1), 014010. https://doi.org/10.1088/1748-9326/ac3ced.
Wang, K., Onodera, S.I., Saito, M., Ishida, T., 2022c. Assessment of long-term phosphorus budget changes influenced by anthropogenic factors in a coastal catchment of Osaka Bay. *Sci. Total Environ.* 843, 156833. https://doi.org/10.1016/j.scitotenv.2022.156833.
Wang, K., Onodera, S.I., Saito, M., Shimizu, Y., 2024. Assessment of nitrogen budget in detailed spatial pattern using high precision modeling approach with constructed accurate agricultural behavior. *Sci. Total Environ.* 912, 169631. https://doi.org/10.1016/j.scitotenv.2023.169631.
Watson, F.G.R., Vertessy, R.A., Grayson, R.B., 1999. Large-scale modelling of forest hydrological processes and their long-term effect on water yield. Hydrol. Process. 13 (5), 689–700. https://doi.org/10.1002/(SICI)1099-1085(19990415)13:5<689::AID-HYP773>3.0.CO;2-D.
Yang, Q., Zhang, X., 2016. Improving SWAT for simulating water and carbon fluxes of forest ecosystems. Sci. Total Environ. 569–570, 1478–1488. https://doi.org/10.1016/j.scitotenv.2016.06.238.
Yang, Y., Roderick, M.L., Guo, H., Miralles, D.G., Zhang, L., Fatichi, S., Yang, D., 2023. Evapotranspiration on a greening Earth. Nat. Rev. Earth Environ. 4 (9), 626–641. https://doi.org/10.1038/s43017-023-00464-3.
Yao, Y., Ciais, P., Joetzjer, E., Li, W., Zhu, L., Wang, Y., Viovy, N., 2024. The impacts of elevated CO_2 on forest growth, mortality, and recovery in the Amazon rainforest. Earth Syst. Dyn. 15 (3), 763–778. https://doi.org/10.5194/esd-15-763-2024.
Yuan, M., Gan, G., Bu, J., Su, Y., Ma, H., Liu, X., Gao, Y., 2024. Comparative evaluation of four actual evapotranspiration models over different ecosystems and climate zones in China. J. Water Clim. Change, jwc2024724. https://doi.org/10.2166/wcc.2024.724.
Zhang, Y., Kong, D., Gan, R., Chiew, F.H., McVicar, T.R., Zhang, Q., Yang, Y., 2019. Coupled estimation of 500 m and 8-day resolution global evapotranspiration and gross primary production in 2002–2017. Remote Sens. Environ. 222, 165–182. https://doi.org/10.1016/j.rse.2018.12.031.
Zhao, W., Tan, W., Li, S., 2021. High leaf area index inhibits net primary production in global temperate forest ecosystems. Environ. Sci. Pollut. Res. 28, 22602–22611. https://doi.org/10.1007/s11356-020-11928-0.